

# Quantum well intrasubband photodetector for far infrared and terahertz radiation detection

David Z.-Y. Ting,<sup>a)</sup> Yia-Chung Chang,<sup>b)</sup> Sumith V. Bandara, and Sarath D. Gunapala  
*Jet Propulsion Laboratory, California Institute of Technology, Pasadena, California 91109*

(Received 22 March 2007; accepted 20 July 2007; published online 14 August 2007)

The authors present a theoretical analysis on the possibility of using the dopant-assisted intrasubband absorption mechanism in quantum wells for normal-incidence far infrared/terahertz radiation detection. The authors describe the proposed concept of the quantum well intrasubband photodetector (QWISP), which is a compact semiconductor heterostructure device compatible with existing GaAs focal-plane array technology, and present theoretical results demonstrating strong normal-incidence absorption and responsivity in the QWISP. © 2007 American Institute of Physics. [DOI: 10.1063/1.2770766]

Far infrared (FIR)/terahertz radiation detection has been demonstrated in compact semiconductor heterostructure devices such as the quantum cascade detector (QCD),<sup>1</sup> the heterojunction interfacial work function internal photoemission (HEIWIP) detector,<sup>2,3</sup> and the quantum well infrared photodetector (QWIP).<sup>4</sup> These devices exploit intersubband absorption (QCD and QWIP), or bulk intraband free carrier absorption (HEIWIP). In this work, we present a theoretical analysis on the possibility of using intrasubband absorption in quantum wells for FIR/terahertz detection, and propose the quantum well intrasubband photodetector (QWISP) device concept based on this mechanism.

We introduce the QWISP by comparing it with a QWIP; both devices are illustrated in Fig. 1. The FIR/terahertz QWIP has a wide quantum well for the small intersubband transition energy, and a low barrier to keep the upper state in resonance with the top of the barrier in accordance with the bound-to-quasibound QWIP design rule.<sup>5</sup> Because the ground-state energy is very close to the top of the barrier, to limit dark current, FIR/terahertz QWIPs require low doping, which leads to low quantum efficiency.<sup>4</sup> The QWISP addresses this problem by using the intrasubband absorption mechanism instead. In a study of discrete dopant effects in long-wavelength infrared (LWIR) QWIP, we found that dopant impurity scattering could induce large normal-incidence FIR absorption.<sup>6</sup> However, this effect cannot be exploited in LWIR QWIPs because the electrons photoexcited via intrasubband transitions do not have sufficient energy to escape from the well to contribute to photocurrent. The QWISP, illustrated in Fig. 1(b), can be viewed as a modified LWIR QWIP where the barrier has been lowered to allow the electrons photoexcited by FIR/terahertz radiation through intrasubband absorption to escape into the continuum and carry current. The intrasubband absorption process does not conserve momentum (or  $\mathbf{k}_{\parallel}$ ). Moreover, the excited carrier extraction process also requires momentum change. Suppose an electron is photoexcited from the Fermi sea to a state with energy  $E_1(\mathbf{k}_{\parallel})$  above the barrier, as illustrated in Fig. 1(b). Due to energy dispersion in the barrier itself, the excited electron would still see a tunneling barrier of

$[E_b(\mathbf{k}_{\parallel}) - E_1(\mathbf{k}_{\parallel})]$  that hampers it from escaping without further scattering. We will show that elastic scattering by dopants in the quantum well can provide the momentum scattering necessary for both intrasubband absorption and photoexcited carrier escape. In our calculations, we take the view that  $\mathbf{k}_{\parallel}$  is no longer a good quantum number under the influence of the random dopant potential, and the quantum well states are spread out in  $k$  space. It is this  $k$ -space smearing that enables intrasubband absorption and excited carrier extraction. Consider, for example, an intrasubband transition where the upper state energy is slightly above the barrier band edge. Loosely speaking,  $k$ -space smearing means that this upper state effectively sees a range of barrier heights  $E_b(k_{\parallel})$  corresponding to the span of different  $k_{\parallel}$ 's. The taller barriers serve to confine the state in the well (necessary for good oscillator strength), and the lower barriers [with  $E_b(k_{\parallel}) < E$ ] allow for escape into the barrier for photo-carrier extraction. Note that the dopant potential determines the degree of  $k$ -space smearing ( $\Delta k_{\parallel}$ ) and hence the energy scale ( $\Delta E$ ) involved; they in turn control the QWISP characteristics.

Strong intrasubband absorption requires high doping levels, which can be used without significant dark current penalties so long as the activation energy ( $E_a = E_b - E_F$ ; see

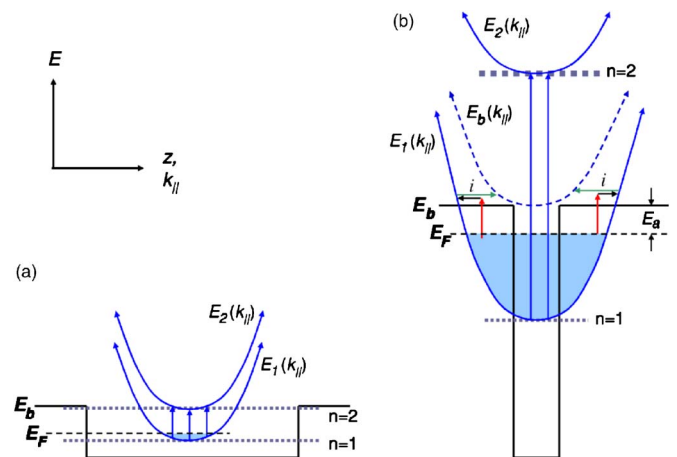


FIG. 1. (Color online) Schematic illustrations of the energy dispersions and energy band diagrams of (a) FIR/terahertz QWIP; (b) QWISP showing intrasubband and impurity scattering assisted intrasubband optical absorption and carrier extraction mechanisms.

<sup>a)</sup>Electronic mail: david.z.ting@jpl.nasa.gov

<sup>b)</sup>Permanent address: Department of Physics, University of Illinois at Urbana-Champaign, Urbana, IL 61801.

TABLE I. GaAs/AlGaAs QWIP (set P) and QWISP (set S) structure and simulation parameters, and calculated activation energies and responsivity peak positions.

	$L_W$ (Å)	$L_B$ (Å)	Al%	$n_D$ ( $10^{18}$ cm $^{-3}$ )	$\tau_{\text{life}}$ (ps)	$\tau_{\text{relax}}$ (ps)	$F$ (V/cm)	$E_a$ (meV)	$\lambda_{\text{peak}}$ ( $\mu\text{m}$ )
P1	119	552	5.0	0.1	10	200	3000	33.9	34
P2	155	702	3.0	0.06	10	350	600	19.9	57
P3	221	951	1.5	0.03	10	700	120	9.4	111
S1	50	552	15.9	5.0	5	50	3000	33.8	37
S2	50	702	14.2	5.0	5	50	600	20.6	58
S3	50	951	12.8	5.0	5	50	120	9.7	109

Fig. 1) is sufficiently large. In modeling the QWISP with high dopant densities, for which multiple scattering is important and perturbation theory may be inadequate, we use a three-dimensional (3D) supercell approach that is analogous to the rigorous coupled wave analysis method<sup>7</sup> for treating optical waves in complex geometries. The system is described by a one-band effective mass equation with an anisotropic energy-dependent effective mass used to model the nonparabolic conduction band dispersion of the  $\Gamma$  valley. Under high doping conditions, the impurity states can merge with the conduction subband, and it is important to include exchange-correlation effect induced band gap renormalization,<sup>8</sup> which, along with band nonparabolicity, can cause Fermi level lowering that is substantial relative to the wavelengths of interest. Band structure effects on optical matrix elements are included perturbatively using a 14-band  $k \cdot p$  method based formulation.<sup>9</sup> The effects of discrete dopant impurities are incorporated as screened Coulomb potentials, similar to the technique used in Ref. 10. It is important to describe the continuum states just above the barriers in the QWISP. We model this by computing the quasicontinuum states in an extended barrier region surrounded by a slightly taller artificial barrier. More details on the method are described elsewhere.<sup>6</sup> Once we obtain the energy levels and wave functions, properties such as absorption coefficient and responsivity can be computed via standard methods,<sup>11,12</sup> appropriately adapted for the supercell geometry.

Simulation parameters for the FIR/terahertz QWIPs and QWISPs with GaAs wells and AlGaAs barriers are listed in Table I. The QWIP structures, including well width ( $L_W$ ), barrier width ( $L_B$ ), barrier composition (Al%), and well doping density ( $n_D$ ) are taken from the literature.<sup>4</sup> The QWISPs have identical well widths and doping densities, but different barriers. The correspondingly numbered QWIP and QWISP devices have approximately the same barrier widths and activation energies ( $E_a$ ) to keep their tunneling and thermal emissive dark currents on par. The QWIP results are obtained using a simple one-dimensional calculation, since impurity scattering effects on optical properties are not significant at low doping densities. For the QWISPs, we use 600 Å lateral periodicity supercells containing 90 random impurities to simulate random dopant potential effects. In all cases, the doping densities are sufficiently high so that the impurity band (not shown in Fig. 1) merges with the first conduction subband of the quantum well.<sup>13</sup> We caution that because of small energy scales involved and the uncertainties in the simulation, the parameters in Table I should be considered as approximate guides rather than precise designs.

Figure 2 shows the computed absorption coefficients for the quantum well regions. The QWIP absorption coefficients are from intersubband transitions, induced by side-incidence

light polarized along the growth direction ( $z$ ). P1, P2, and P3 have absorption peaks at 34, 57, and 109  $\mu\text{m}$ , respectively. The intersubband oscillator strengths for the three QWIP structures are approximately equal. The difference in absorption strengths mainly reflects the fact that lower doping is required in longer wavelength QWIPs to limit the dark current. The QWISP  $z$ -polarized absorptions are due to bound-to-continuum intersubband transitions ( $n=1$  to  $n=2$ ), and appear as broad peaks around 10.0  $\mu\text{m}$ . Of primary interests are the impurity-assisted QWISP intrasubband transitions, for which oscillator strengths are concentrated and enhanced by quantum confinement into the components associated with  $x$ - $y$  polarized radiation, resulting in strong normal-incidence absorption. The normal-incidence absorption spectra for S1, S2, and S3 are similar, with a broad, strong absorption peak centered at 150  $\mu\text{m}$  and dropping off to half height at  $\sim 55$  and  $\sim 470$   $\mu\text{m}$  on the two sides. The peak position suggests that the dopant potential favors scattering events with small  $\Delta k_{\parallel}$ ; therefore the impurity scattering induced intrasubband transitions involve mostly states near the Fermi surface, with  $\Delta E$  in the FIR. These results are in general agreement with theoretical results obtained for  $\delta$ -doped quantum wells.<sup>14</sup>

Table I shows the capture lifetimes ( $\tau_{\text{life}}$ ) and relaxation times ( $\tau_{\text{relax}}$ ; intersubband for QWIP, intrasubband for QWISP) used for responsivity modeling, chosen based on experimental results.<sup>15-17</sup> Longer capture times are used for the QWIPs to account for the lower doping. Compared to the

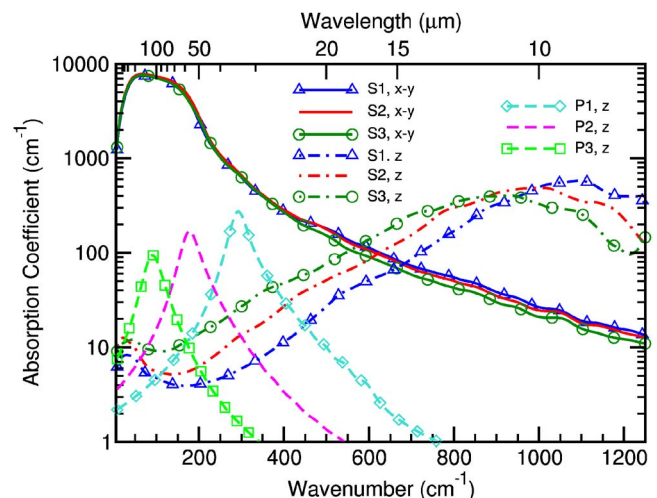


FIG. 2. (Color online) Calculated quantum well absorption coefficients for structures listed in Table I. The QWIP (set P) results are for side-incidence ( $z$ -polarized) radiation only. The QWISP (set S) results for both normal-incidence (averaged over  $x$  and  $y$  polarizations) and side-incidence ( $z$ ) radiations are shown.

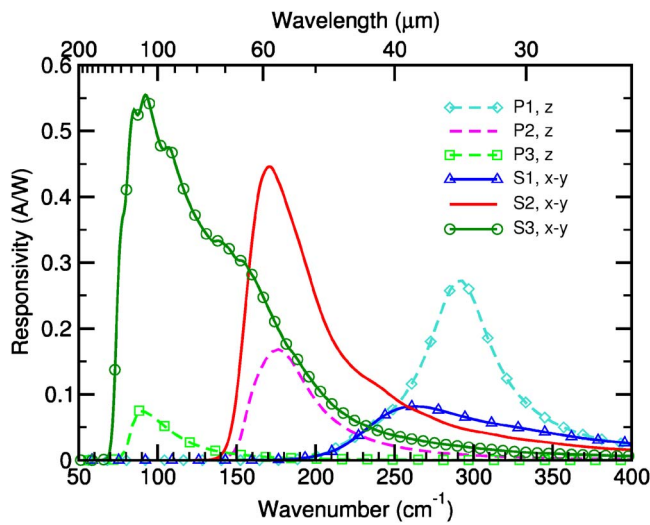


FIG. 3. (Color online) Low-temperature FIR/terahertz QWIP (set P) side-incidence responsivity and QWISP (set S) normal-incidence responsivity. Modeling parameters are listed in Table I.

QWIP, tunneling escape lifetimes are much longer for the QWISP due to the presence of the tunneling barrier  $[E_b(\mathbf{k}_{\parallel}) - E_1(\mathbf{k}_{\parallel})]$  mentioned earlier. For instance, the typical zero-bias tunneling escape times for QWISP states just above the barrier is estimated from transmission resonance width calculations to be  $\sim 5$  ps, while the escape time for the QWIP is estimated from impact frequency and barrier transparency to be  $\sim 5$  fs.<sup>12</sup> Because of the small transition energies (below LO phonon energy) and low operating temperatures, long relaxation times are expected since acoustic phonon emission is the primary energy relaxation mechanism. For the QWISP we used a 50 ps intrasubband relaxation time, based on the measured low-temperature ( $< 35$  K) intrasubband electron cooling times in quantum wells.<sup>15,17</sup> Note that since the intrasubband relaxation times is considerably shorter at higher temperature ( $\sim 100$  fs), the QWISP is limited to low-temperature operation. Smaller applied electric fields ( $F$ ) are used for structures with lower activation energies to limit dark current.<sup>4</sup> Figure 3 shows the computed responsivities. The side-incidence QWIP responsivity peaks are found at the same positions as the absorptions peaks. The QWISP side-incidence FIR response is negligible, and is not shown. The QWISP normal-incidence responsivity peak positions are determined by the activation energies (see Table I). Figure 3 shows the complementary nature of the QWIP and the QWISP. Due to the limited range of impurity scattering in  $k$ -space ( $\Delta k_{\parallel}$ ), the QWISP is ineffective in the LWIR where the QWIP performs well. But the QWISP has strong (normal incidence) response in the FIR where QWIP shows diminished performance due to lower doping.

It is also interesting to compare the QWISP concept with the  $n$ -type HEIWIP, which has recently demonstrated excellent FIR performance.<sup>3</sup> In contrast to the QWIP and the QCD, both the QWISP and the HEIWIP are normal-incidence detectors. The HEIWIP uses 3D intraband absorption, which has equal oscillator strengths for normal- and side-incident radiation. The QWISP uses two-dimensional

(2D) intrasubband absorption, which has enhanced normal incidence but negligible side-incidence FIR oscillator strengths. Excited carrier extraction in HEIWIP is 3D to 3D through the escape cone,<sup>18</sup> in QWISP it is 2D to 3D, and is enabled by dopant impurity scattering. The HEIWIP has essentially unity gain, while the QWISP uses a multi-quantum-well structure, and therefore has subunity gain like the QWIP. There is considerable flexibility in the QWISP design, where the same activation energy can be obtained through different combinations of well widths, barrier height, and doping levels. The QWISP does not require the use of low barriers (e.g., AlGaAs with very low Al fraction), and in general, higher doping density results in increased response. Note that quantum wells with different doping levels or well widths could be integrated into the same device to tailor the response spectrum. Finally, we note that the QWISP can be built upon existing mature QWIP technology, and provides a possible pathway to large-format far-IR focal-plane arrays.

The authors thank R. Q. Yang and X. Cartoixa for helpful discussions, and thank the reviewer for stimulating the discussion on the escape mechanism in the QWISP and comparison with HEIWIP. The research described in this letter was carried out at the Jet Propulsion Laboratory, California Institute of Technology, through an agreement with NASA.

- <sup>1</sup>M. Graf, G. Scalari, D. Hofstetter, J. Faist, H. Beere, E. Linfield, D. Ritchie, and G. Davies, *Appl. Phys. Lett.* **84**, 475 (2004).
- <sup>2</sup>A. G. U. Perera, S. G. Matsik, B. Yaldiz, H. C. Liu, A. Shen, M. Gao, Z. R. Wasilewski, and M. Buchanan, *Appl. Phys. Lett.* **78**, 2241 (2001).
- <sup>3</sup>A. B. Weerasekera, M. B. M. Rinzan, S. G. Matsik, A. G. U. Perera, M. Buchanan, H. C. Liu, G. von Winckel, A. Stintz, and S. Krishna, *Infrared Phys. Technol.* **50**, 194 (2007).
- <sup>4</sup>H. Luo, H. C. Liu, C. Y. Song, and Z. R. Wasilewski, *Appl. Phys. Lett.* **86**, 231103 (2005).
- <sup>5</sup>S. D. Gunapala and K. M. S. V. Bandara, *Physics of Thin Films* (Academic, New York, 1995), Vol. 21, p. 113.
- <sup>6</sup>D. Z.-Y. Ting, Y.-C. Chang, S.-V. Bandara, C. J. Hill, and S. D. Gunapala, *Infrared Phys. Technol.* **50**, 136 (2007).
- <sup>7</sup>M. G. Moharam, Eric B. Grann, Drew A. Pomet, and T. K. Gaylord, *J. Opt. Soc. Am. A* **12**, 1068 (1995).
- <sup>8</sup>See, M. Helm, in *Intersubband Transition in Quantum Wells: Physics and Device Applications I*, Semiconductors and Semimetals Vol. 62, edited by H. C. Liu and F. Capasso (Academic, New York, 2000), Chap. 1, pp. 1–99.
- <sup>9</sup>C. W. Cheah, L. S. Tan, and G. Karunasiri, *J. Appl. Phys.* **91**, 5105 (2002).
- <sup>10</sup>G. D. Sanders and Y.-C. Chang, *Phys. Rev. B* **35**, 1300 (1987).
- <sup>11</sup>Y.-C. Chang, J. Cheung, A. Chiou, and M. Khoshnevisan, *J. Appl. Phys.* **68**, 4233 (1990).
- <sup>12</sup>H. C. Liu, in *Intersubband Transition in Quantum Wells: Physics and Device Applications I*, Semiconductors and Semimetals Vol. 62, edited by H. C. Liu and F. Capasso (Academic, New York, 2000), Chap. 3, pp. 126–196.
- <sup>13</sup>M. Carras, V. Berger, X. Marcadet, and B. Vinter, *Phys. Rev. B* **70**, 233310 (2004).
- <sup>14</sup>C. Steen, C. Metzner, M. Hoffmann, and G. H. Döhler, *Physica E (Amsterdam)* **7**, 220 (2000).
- <sup>15</sup>S. R. Schmidt, A. Seilmeier, and H. C. Liu, *J. Appl. Phys.* **91**, 5545 (2002).
- <sup>16</sup>B. N. Murdin, W. Heiss, C. J. G. M. Langerak, S.-C. Lee, I. Galbraith, G. Strasser, E. Gornik, M. Helm, and C. R. Pidgeon, *Phys. Rev. B* **55**, 5171 (1997).
- <sup>17</sup>S. Lutgen, R. A. Kaindl, M. Woerner, T. Elsaesser, A. Hase, and H. Künzel, *Phys. Rev. B* **54**, R17343 (1996).
- <sup>18</sup>J. M. Mooney and J. Silverman, *IEEE Trans. Electron Devices* **32**, 33 (1985).